

Experimental demonstration of quantum causal inference via noninvasive measurements

Hongfeng Liu,^{1,*} Xiangjing Liu,^{2,3,4,1,*} Qian Chen,⁵ Yixian Qiu,⁴ Vlatko Vedral,⁶ Xinfang Nie,^{1,7,†} Oscar Dahlsten,^{8,1,9,10,‡} and Dawei Lu^{1,9,7,11,§}

¹Department of Physics, Southern University of Science and Technology, Shenzhen 518055, China

²CNRS@CREATE, 1 Create Way, 08-01 Create Tower, Singapore 138602, Singapore

³MajuLab, CNRS-UCA-SU-NUS-NTU International Joint Research Unit, Singapore

⁴Centre for Quantum Technologies, National University of Singapore, Singapore 117543, Singapore

⁵Univ Lyon, Inria, ENS Lyon, UCBL, LIP, F-69342, Lyon Cedex 07, France

⁶Clarendon Laboratory, University of Oxford, Parks Road, Oxford OX1 3PU, United Kingdom

⁷Quantum Science Center of Guangdong-Hong Kong-Macao Greater Bay Area, Shenzhen 518045, China

⁸Department of Physics, City University of Hong Kong, Tat Chee Avenue, Kowloon, Hong Kong SAR, China

⁹Shenzhen Institute for Quantum Science and Engineering, Southern University of Science and Technology, Shenzhen 518055, China

¹⁰Institute of Nanoscience and Applications, Southern University of Science and Technology, Shenzhen 518055, China

¹¹International Quantum Academy, Shenzhen 518055, China

(Dated: November 12, 2024)

We probe the foundations of causal structure inference experimentally. The causal structure concerns which events influence other events. We probe whether causal structure can be determined without intervention in quantum systems. Intervention is commonly used to determine causal structure in classical scenarios, but in the more fundamental quantum theory, there is evidence that measurements alone, even coarse-grained measurements, can suffice. We demonstrate the experimental discrimination between several possible causal structures for a bipartite quantum system at two times, solely via coarse-grained projective measurements. The measurements are implemented by an approach known as scattering circuits in a nuclear magnetic resonance platform. Using recent analytical methods the data thus gathered is sufficient to determine the causal structure. Coarse-grained projective measurements disturb the quantum state less than fine-grained projective measurements and much less than interventions that reset the system to a fixed state.

Introduction.—Determining the causal structure, i.e. which variables influence others, is known as causal inference [1, 2]. Causal inference is, for example, important in understanding medical trials [3, 4], and has a range of machine learning applications [5, 6]. Reichenbach’s Common Cause Principle identifies causal structures that may underly probabilistic correlations. The principle states that when there is a probabilistic correlation between two events, A and B , this correlation can be explained by one of the following causal relationships: (i) A is a cause of B , (ii) B is a cause of A , (iii) there is a third common cause, C , that influences both A and B . There can also, by inspection, be a combination of a common cause and causal influence between A and B . The resulting five types of causal structures are depicted in Fig. 1. Determining the causal structure can in principle be undertaken via *intervening* in the system [2, 3] to see how the probability distribution is altered. Partial causal structure inference from observations, without interventions, is sometimes possible [2, 4, 7].

Causal structure inference is also being investigated in the more fundamental quantum level [8–23]. Causal inference via interventions, in particular resetting the state of the quantum system, have been considered [24–32]. It has been realized that, at least in some cases, such resets are not necessary to determine the causal structure and that measurements can suffice [11, 24, 33]. For instance, a quantum signature for temporal correlation based on observations can rule out the common cause mechanism [11]. Further, an observational scheme is proposed to infer quantum causal structure in Ref. [24], for the case of a common cause represented by a correlated pure state and causal influence via a unitary channel. Reichenbach’s

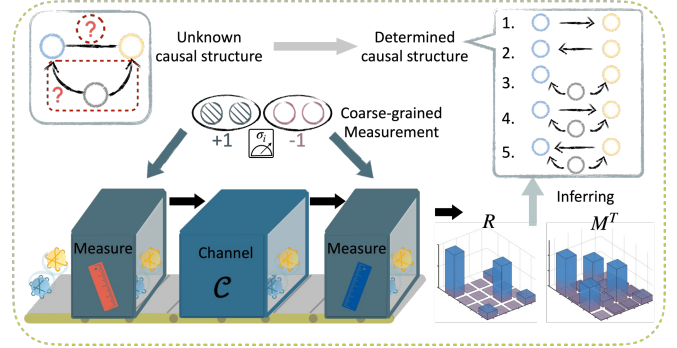


FIG. 1. **Overview of experiment and theoretical analysis.** It is unknown to the experimenter which quantum system is influencing which, and whether there are correlations in the initial state, termed a common cause. For example, structure 4 corresponds to correlations in the initial state followed by a channel whereby the blue system influences the yellow system. Data is taken from binary coarse-grained measurements on the initial state and after the channel. The data is turned into a pseudo density matrix R and associated Choi matrix M^T , from which the causal structure is inferred.

principle has been extended to the quantum case [16] and the differences between quantum and classical causality have been studied from a resource theory perspective [34]. Partial causal inference from observations in the quantum case has been analysed in terms of sets of bounds on correlations [35]. These promising results together suggest it is possible to extend causal inference to the quantum case, and that there may be a significant difference to the classical case in that measure-

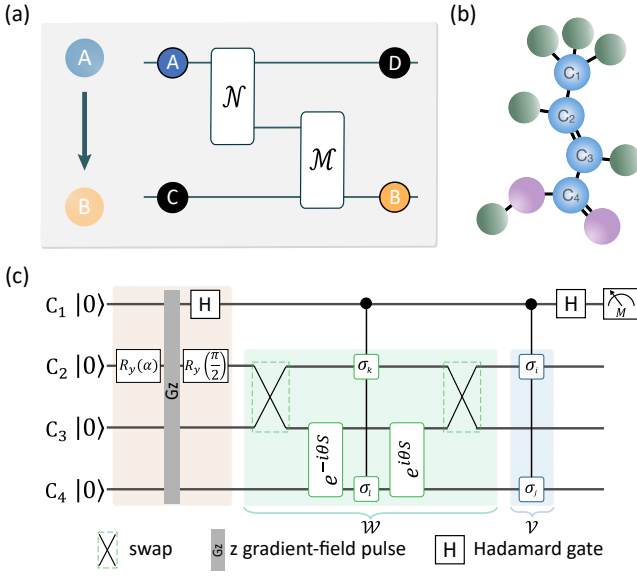


FIG. 2. **Experimental setup.** (a) The causal structure (left) and the circuit model (right). The directed acyclic graph represents the causal structure, where the nodes mean quantum systems and the directed edge means causal influence. The circuit model represents the channel evolution of the quantum system at different time nodes. (b) Molecular structure of the four-qubit NMR quantum processor consisting of four ^{13}C spins. (c) Experimental quantum circuit for measuring the expectation values $\langle \sigma_i^A \sigma_j^C, \sigma_k^D \sigma_l^E \rangle$.

ments alone can suffice. A key question is how far one can push this in terms of causal inference from (projective) measurements alone. Ideally, one wants causal inference schemes that are experimentally viable, are minimally invasive, and come together with clear data analysis.

Here, we provide the experimental demonstration of a quantum causal inference protocol that is highly non-invasive. The experiments were undertaken on an NMR platform. As shown in FIG. 1, the observer gains data from observing two quantum systems A and B at two times. The observer wants to know the causal structure of the process generating the data. The causal inference scheme employs no reset-type interventions but rather only coarse-grained projective measurements. These measurements are implemented by a method termed scattering circuits [36, 37]. The measurement data is analysed via the pseudo-density matrix (PDM) formalism, a space-time state formalism in which one assigns a PDM to the data table of experiments involving measurements on systems at several times [11, 38]. In the data analysis, firstly one identifies whether there is negativity in certain reduced states of the PDM. Then one evaluates the time-asymmetry of the PDM. Through this combination of experimental and analytical methods, we demonstrate causal inference from highly non-invasive measurements on a bipartite quantum system at two times. We expand on the results in the accompanying Ref. [39].

Quantum causal inference task of five possible structures.— The observer has data from observing two quantum systems

A and B . The observer wants to know the causal structure generating the data. In line with Reichenbach’s principle, we allow for five causal structures that are to be distinguished (see FIG. 1). These structures are distinguished by the direction of any causal influence between A and B , and by whether there are initial correlations or not. Scenarios with causal influence in both directions (loops), such as global unitaries on A and B are excluded, such that there is a well-defined causal direction [1, 2]. The observer aims to identify which of these potential causal structures is applicable in the given scenario. **Exploiting space-time states and time asymmetry for causal inference.**— Our protocol builds on the Pseudo-Density Matrix (PDM) formalism, which generalizes the conventional density matrix by assigning a Hilbert space to each instant in time [11, 38, 40–43]. Recall that the standard density matrix for n qubits can be written as a linear combination of n -qubit basis matrices $\sigma_i \in \{\mathbb{1}, \sigma_x, \sigma_y, \sigma_z\}^{\otimes n}$ and that the coefficients then correspond, up a factor, to the expectation value of the given σ_i . The PDM formalism uses the same expansion to represent experiments at several times.

The 2-time n -qubit PDM is defined as:

$$R_{12} = \frac{1}{2^{2n}} \sum_{i_1, i_2=0}^{4^n-1} \langle \sigma_{i_1}, \sigma_{i_2} \rangle \sigma_{i_1} \otimes \sigma_{i_2}, \quad (1)$$

where $\sigma_{i_\alpha} \in \{\mathbb{1}, \sigma_x, \sigma_y, \sigma_z\}^{\otimes n}$ is an n -qubit Pauli matrix at time t_α , $\alpha = 1, 2$ and $\langle \sigma_{i_1}, \sigma_{i_2} \rangle$ denotes the expectation value of the product of observables σ_{i_1} at t_1 and σ_{i_2} at t_2 . These expectation values can be measured by coarse-grained measurements which involve n qubits and 2 times.

The PDM can have negative eigenvalues, which indicate temporal correlations (causal influence). The negativity of a square matrix O can be quantified [11] by the measure:

$$f(O) := \text{Tr} \sqrt{OO^\dagger} - \text{Tr} O. \quad (2)$$

$f(O) > 0$ when O has negative eigenvalues, and $f(O) = 0$ when O is positive semidefinite. $f(R) > 0$ indicates the PDM is associated with multiple times.

To determine the temporal ordering we compare the PDM as given by the experimental data, without time labels, with the time-reversed PDM [33]. The time-reversed PDM,

$$R_{21} := S R_{12} S^\dagger, \quad (3)$$

where S denotes the operator that swaps the systems at times t_1 and t_2 . From the PDM we can derive a matrix representation of the channel in question known as a Choi matrix M^T [33, 38]. This matrix M^T is positive exactly if the channel is an allowed channel in a certain sense. Comparing the M^T matrices for the given PDM and the time-reversed PDM can reveal that only one temporal ordering assignment is allowed.

The following table summarises the assignment of causal structure as a function of the negativity of the experimentally determined matrices R and M^T [38].

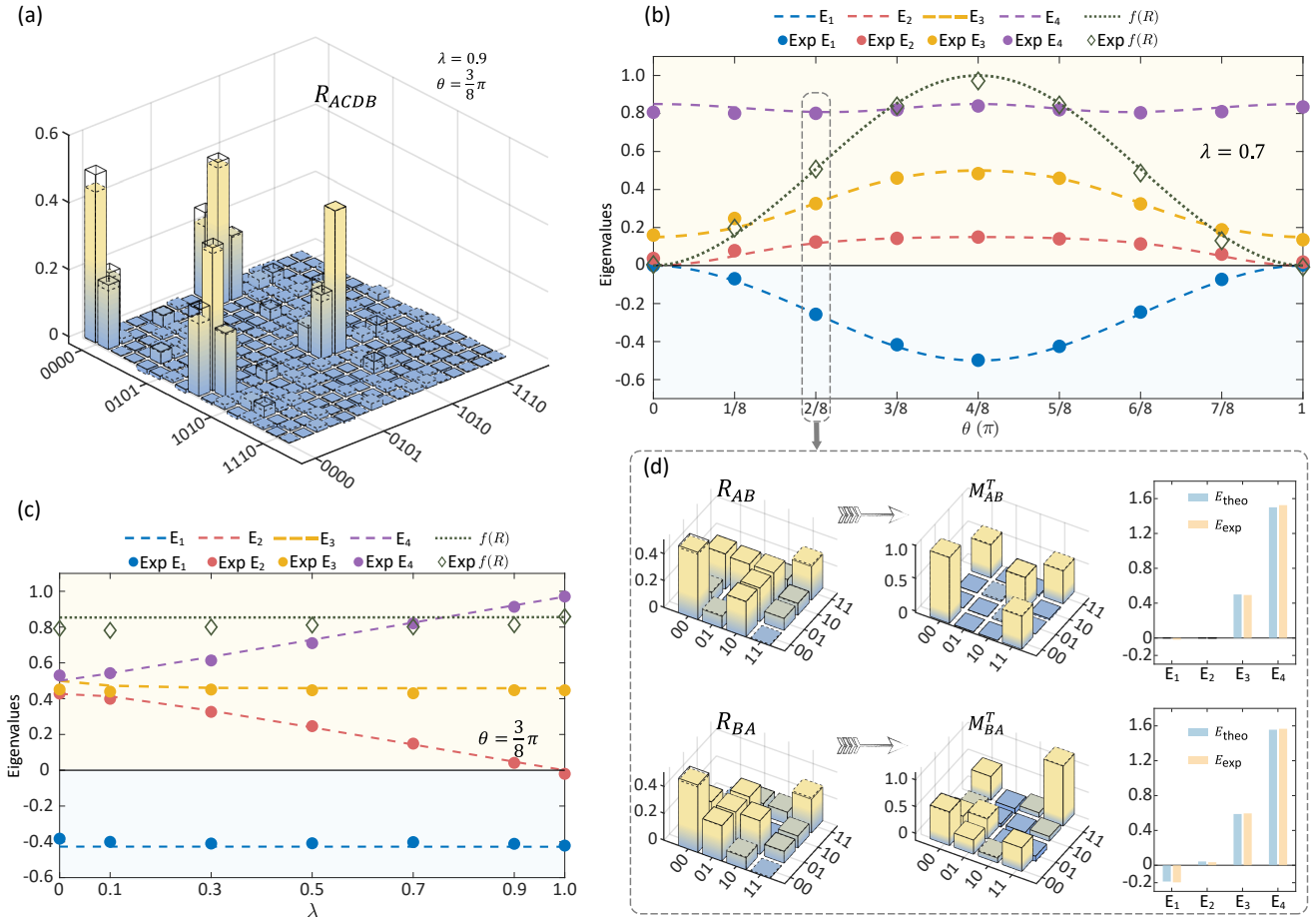


FIG. 3. **Experimentally acquired data for causal inference highly consistent with theoretical predictions.** (a) The full PDM R_{ACDB} for $\lambda = 0.9$ and $\theta = 3\pi/8$. The solid bars represent the theoretical prediction, while the color bars with dashed lines indicate the experimentally acquired values. (b) The 4 eigenvalues of the reduced PDM R_{AB} for different θ . E_1 to E_4 are the theoretical predictions whilst Exp E_1 to Exp E_4 are inferred from experimental data. The negativity of the PDM $f(R)$ is also shown similarly. (c) is the same as (b) except for the x-axis being the initial state parameter λ . In (b) $\lambda = 0.7$, and in (c) the $\theta = 3\pi/8$; the error bars are within the size of the marker symbols (see Ref. [39]). (d) The experimentally measured reduced PDMs R_{AB} and R_{BA} are shown together with the corresponding inferred Choi matrices M^T . The eigenvalues of the Choi matrices are shown next to their experimental predictions, where the $\lambda = 0.7$ and $\theta = 2\pi/8$.

$f(R_{AB})$	$f(M_{AB}^T)$	$f(M_{BA}^T)$	R_{AB} is compatible with
0	Any	Any	Common Cause
> 0	0	> 0	$A \rightarrow B$
> 0	> 0	0	$B \rightarrow A$
> 0	0	0	$A \rightarrow B$ or $B \rightarrow A$
> 0	> 0	> 0	Mixture

Experimental approach via nuclear spins and scattering circuits.— We now describe the experimental implementation of the quantum causal inference protocol on a four-qubit NMR quantum processor [44], depicted in Fig. 2(b).

To implement the light touch measurements that give the data, we use what is known as a quantum scattering circuit [36, 45, 46] to obtain the expectation values of Eq. (1) as depicted in Fig. 2. We prove in Ref. [39] that these circuits indeed give the correct expectation values. The first of the four qubits acts as the probe, the second and fourth qubits as the quantum systems of interest, and the third qubit as an

ancillary system.

We perform two sets of experiments, one set for unitary time evolution and one set for a completely decoherent evolution.

Unitary evolution of unknown causal structure.— We acquired sufficient experimental data to reconstruct the full PDM R_{ACDB} . The purpose is to test that the theoretical model matches the experimental data. (The causal inference does not require the full PDM.) For $\lambda = 0.9$ and $\theta = \frac{3\pi}{8}$, we measured the σ_z expectation value of the probe qubit, $\langle \sigma_z \rangle_{\text{probe}}$, by going through the complete set of Pauli operators on A, B, C and D . This data enabled us to construct the experimental PDM R_{ACDB} , as shown in Fig. 3(a). The agreement between the experimental results and theory predictions is high as demonstrated in Fig. 3.

We investigated the reduced PDM R_{AB} for a range of parameters. We set $\sigma^C = \sigma^D = \mathbb{1}$ since the reduced PDM R_{AB} is

sufficient for our quantum causal inference protocol. We collected the data $\langle \sigma_z \rangle_{\text{probe}}$ for R_{AB} in two scenarios: (i) fixing the polarization parameter λ in the initial state while varying the channel parameter θ , and (ii) fixing the channel parameter θ while varying the polarization parameter λ . Firstly, we set $\lambda = 0.7$ and then systematically varied the channel parameter θ over the range from 0 to π . After constructing R_{AB} , its eigenvalues E_i and negativity $f(R_{AB})$ are depicted in Fig. 3(b). We observe that $f(R_{AB}) > 0$ except for two extreme values $\theta = 0$ and $\theta = \pi$, where the channel \mathcal{M} becomes trivial, i.e., $e^{-i\theta S} = \mathcal{I}$. Secondly, we varied the polarization parameter λ while fixing θ at $3\pi/8$. The eigenvalues E_i and negativity $f(R)$ of the experimentally constructed R_{AB} are depicted in Fig. 3(c). A non-zero constant $f(R)$ is observed despite the initial state change. In both scenarios, one can indeed certify the causal structure solely based on the observed data R_{AB} .

The next step of the protocol is to calculate the Choi matrices of the process and its time reverse from the experimental PDMs when $f(R) > 0$ but the time order is unknown. More precisely, we let $\lambda = 0.7$ and $\theta = \pi/4$. Based on the two constructed PDMs R_{AB} and R_{BA} , we calculated the corresponding Choi matrices M_{AB}^T and M_{BA}^T (see Ref. [39]) and then checked the positivity of the Choi matrices. The results are displayed in Fig. 3(d). $f(M_{AB}^T) = 0$ and $f(M_{BA}^T) > 0$ indicate that the data R_{AB} is compatible with the cause-effect mechanism in which A is the cause and B is the effect.

Fully decohering channel of unknown causal structure.— We further applied our causal inference protocol to the cause-effect mechanism where the functional relation of the quantum systems is a fully decohering channel. This experiment probed whether employing coarse-grained measurements alone for causal inference also works when the evolution is, in a sense, classical. The corresponding circuit for constructing the PDM R_{AB} and the experimental details are given in Ref. [39]. The experimental results are shown in Fig. 4.

The fully decohering channel is designed to be the measure-and-prepare channel, i.e., measuring A and then preparing the results on B . The corresponding channel is given by

$$\mathcal{L}(\rho_{AB}) = \langle 0|\rho_A|0\rangle|00\rangle_{AB}\langle 00| + \langle 1|\rho_A|1\rangle|11\rangle_{AB}\langle 11|. \quad (4)$$

In our experiment, we have set $\rho_A = (1 - \lambda)\frac{\mathbb{I}}{2} + \lambda|+\rangle\langle +|$ and $\rho_B = |0\rangle\langle 0|$. Upon obtaining the data $\langle \sigma_i^A \sigma_j^B \rangle$ for various λ , we experimentally constructed the PDMs R_{AB} .

Following our causal inference protocol, we first calculated the eigenvalues E_i and negativities $f(R_{AB})$. The results are depicted in Fig. 4(a). We observe negative eigenvalues in R_{AB} except for $\lambda = 0$. The negativity rules out the common-cause mechanism. We then proceeded to determine the cause and effect. We extract the Choi matrices M_{AB}^T and M_{BA}^T from R_{AB} and R_{BA} , respectively. We also calculated their negativities. The results are shown in Fig. 4(b-d). We observe that for all λ , M_{AB}^T is positive while M_{BA}^T has negative eigenvalues. Combining the above, we conclude that the causal structure is $A \rightarrow B$ for $\lambda \neq 0$.

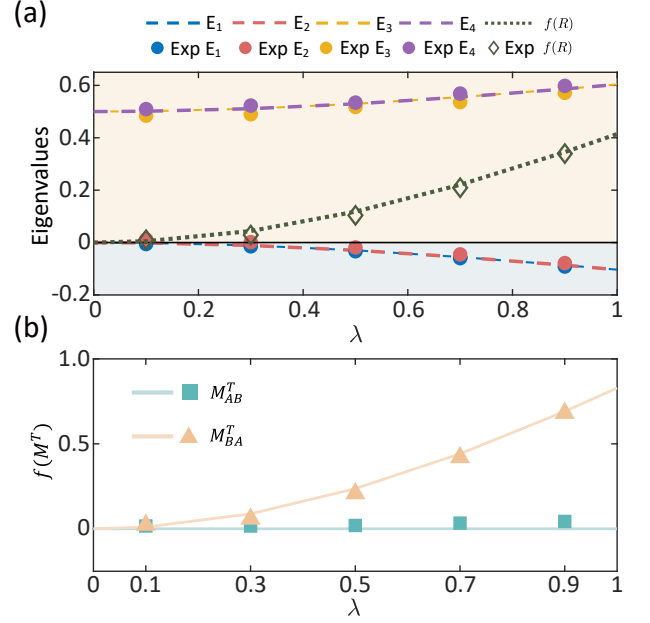


FIG. 4. **Causal inference for fully decohering channel.** (a) The experimental results of the eigenvalues of R_{AB} and the values of $f(R)$ vary with λ . The circles and diamonds indicate eigenvalues and $f(R)$ data points obtained from the experiment, respectively, while the dotted lines indicate the relevant theoretical results. As ρ_a transitions from the maximally mixed state to the quantum state $|+\rangle\langle +|$, the magnitude of the negative eigenvalues correspondingly increases. When ρ_a is in the $|+\rangle\langle +|$ state and passes through the decohering channel, the causal strength from A to B is maximized. Conversely, when ρ_a reaches the maximally mixed state, the causal correlation between A and B becomes undetectable. The error bars are within the size of the marker symbols (see Ref. [39]). (b) Experimental results of $f(M_{BA}^T)$ and $f(M_{AB}^T)$ are shown as squares and triangles for different λ . Theoretical predictions are shown as lines.

The protocol fails as expected for $\lambda = 0$, the case corresponding to the classical limit of no initial coherence. For $\lambda = 0$, our protocol incorrectly assigns the common cause mechanism to the data here since $f(R) = 0$. This is because the setup fully returns to the classical case, with the initial state having no coherence in the computational basis. This is consistent with the hypothesis that in classical probability theory, we *cannot* in general distinguish the causal structure purely based on observational data. The difference between the $\lambda = 0$ case and the other cases of initial coherence can be viewed as confirming a quantum advantage in inferring causal structures.

Concluding remarks and Outlook.— A key message is that quantum causal structure can be inferred solely from measurements. The experiments in addition specify the functional relation M_{AB} , describing the intermediate dynamics between the measurements. This approach may thus lead to new types of multiqubit channel tomography protocols based on coarse-grained measurements alone, including learning the Hamiltonian of the system. Further, the approach here allows for cor-

relations between the initial state and the environment, suggesting the approach can be used to design witnesses of non-Markovianity.

Acknowledgements.— This work is supported by the National Key Research and Development Program of China (2019YFA0308100), and the National Natural Science Foundation of China (Grants No.12104213, 12075110, 12204230, 12050410246, 1200509, 12050410245), Science, Technology and Innovation Commission of Shenzhen Municipality (JCYJ20200109140803865), Guangdong Innovative and Entrepreneurial Research Team Program (2019ZT08C044), Guangdong Provincial Key Laboratory (2019B121203002), City University of Hong Kong (Project No. 9610623), The Pearl River Talent Recruitment Program (2019QN01X298), Guangdong Provincial Quantum Science Strategic Initiative (GDZX2303001 and GDZX2200001), and the National Research Foundation, Prime Minister’s Office, Singapore under its Campus for Research Excellence and Technological Enterprise (CREATE) programme. QC is funded within the QuantERA II Programme that has received funding from the European Union’s Horizon 2020 research and innovation programme under Grant Agreement No 101017733 (VERIQ-TAS). YQ is supported by the National Research Foundation, Singapore, and A*STAR under its CQT Bridging Grant and its Quantum Engineering Programme under grant NRF2021-QEP2-02-P05. V.V is supported by the Gordon and Betty Moore and Templeton Foundations.

* These authors contributed equally to this work.

† niexf@sustech.edu.cn

‡ oscar.dahlsten@cityu.edu.hk

§ ludw@sustech.edu.cn

- [1] H. Reichenbach, *The direction of time*, Vol. 65 (Univ of California Press, 1956).
- [2] J. Pearl, *Causality* (Cambridge university press, 2009).
- [3] A. Balke and J. Pearl, Bounds on treatment effects from studies with imperfect compliance, *J. Am. Stat. Assoc.* **92**, 1171 (1997).
- [4] M. Proserpi, Y. Guo, M. Sperrin, J. S. Koopman, J. S. Min, X. He, S. Rich, M. Wang, I. E. Buchan, and J. Bian, Causal inference and counterfactual prediction in machine learning for actionable healthcare, *Nat. Mach. Intell.* **2**, 369 (2020).
- [5] J. Peters, D. Janzing, and B. Schölkopf, *Elements of causal inference: foundations and learning algorithms* (The MIT Press, 2017).
- [6] A. Feder, K. A. Keith, E. Manzoor, R. Pryzant, D. Sridhar, Z. Wood-Doughty, J. Eisenstein, J. Grimmer, R. Reichart, M. E. Roberts, *et al.*, Causal inference in natural language processing: Estimation, prediction, interpretation and beyond, *Trans. Assoc. Comput. Linguist.* **10**, 1138 (2022).
- [7] J. D. Angrist, G. W. Imbens, and D. B. Rubin, Identification of causal effects using instrumental variables, *J. Am. Stat. Assoc.* **91**, 444 (1996).
- [8] A. J. Leggett and A. Garg, Quantum mechanics versus macroscopic realism: Is the flux there when nobody looks?, *Phys. Rev. Lett.* **54**, 857 (1985).
- [9] O. Oreshkov, F. Costa, and Č. Brukner, Quantum correlations with no causal order, *Nat. Commun.* **3**, 1092 (2012).
- [10] Č. Brukner, Quantum causality, *Nat. Phys.* **10**, 259263 (2014).
- [11] J. F. Fitzsimons, J. A. Jones, and V. Vedral, Quantum correlations which imply causation, *Sci. Rep.* **5**, 18281 (2015).
- [12] J. Barrett, R. Lorenz, and O. Oreshkov, Cyclic quantum causal models, *Nat. Commun.* **12**, 885 (2021).
- [13] J. Barrett, R. Lorenz, and O. Oreshkov, Quantum causal models, *arXiv preprint arXiv:1906.10726* (2019).
- [14] L. Hardy, Probability theories with dynamic causal structure: a new framework for quantum gravity, *arXiv preprint gr-qc/0509120* (2005).
- [15] F. Costa and S. Shrapnel, Quantum causal modelling, *New J. Phys.* **18**, 063032 (2016).
- [16] J.-M. A. Allen, J. Barrett, D. C. Horsman, C. M. Lee, and R. W. Spekkens, Quantum common causes and quantum causal models, *Phys. Rev. X* **7**, 031021 (2017).
- [17] Y. Aharonov, S. Popescu, J. Tollaksen, and L. Vaidman, Multiple-time states and multiple-time measurements in quantum mechanics, *Phys. Rev. A* **79**, 052110 (2009).
- [18] X. Liu, D. Ebler, and O. Dahlsten, Thermodynamics of quantum switch information capacity activation, *Phys. Rev. Lett.* **129**, 230604 (2022).
- [19] A. J. Parzygnat and J. Fullwood, From time-reversal symmetry to quantum Bayes’ rules, *PRX Quantum* **4**, 020334 (2023).
- [20] E. Wolfe, A. Pozas-Kerstjens, M. Grinberg, D. Rosset, A. Acín, and M. Navascués, Quantum inflation: A general approach to quantum causal compatibility, *Phys. Rev. X* **11**, 021043 (2021).
- [21] M. Song, V. Narasimhachar, B. Regula, T. J. Elliott, and M. Gu, Causal classification of spatiotemporal quantum correlations, *Phys. Rev. Lett.* **133**, 110202 (2024).
- [22] E. Wolfe, D. Schmid, A. B. Sainz, R. Kunjwal, and R. W. Spekkens, Quantifying Bell: The resource theory of nonclassicality of common-cause boxes, *Quantum* **4**, 280 (2020).
- [23] H. Liu, Z. Liu, S. Chen, X. Nie, X. Liu, and D. Lu, Certifying quantum temporal correlation via randomized measurements: Theory and experiment, *arXiv preprint arXiv:2409.02470* (2024).
- [24] K. Ried, M. Agnew, L. Vermeyden, D. Janzing, R. W. Spekkens, and K. J. Resch, A quantum advantage for inferring causal structure, *Nat. Phys.* **11**, 414 (2015).
- [25] G. Bai, Y.-D. Wu, Y. Zhu, M. Hayashi, and G. Chiribella, Quantum causal unravelling, *npj Quantum Inf.* **8**, 69 (2022).
- [26] G. Chiribella and D. Ebler, Quantum speedup in the identification of cause–effect relations, *Nat. Commun.* **10**, 1 (2019).
- [27] J.-P. W. MacLean, K. Ried, R. W. Spekkens, and K. J. Resch, Quantum-coherent mixtures of causal relations, *Nat. Commun.* **8**, 1 (2017).
- [28] R. Chaves, G. Carvacho, I. Agresti, V. Di Giulio, L. Aolita, S. Giacomini, and F. Sciarrino, Quantum violation of an instrumental test, *Nat. Phys.* **14**, 291 (2018).
- [29] I. Agresti, D. Poderini, B. Polacchi, N. Miklin, M. Gachechiladze, A. Suprano, E. Polino, G. Milani, G. Carvacho, R. Chaves, *et al.*, Experimental test of quantum causal influences, *Sci. Adv.* **8**, eabm1515 (2022).
- [30] M. Gachechiladze, N. Miklin, and R. Chaves, Quantifying causal influences in the presence of a quantum common cause, *Phys. Rev. Lett.* **125**, 230401 (2020).
- [31] R. V. Nery, M. M. Taddei, R. Chaves, and L. Aolita, Quantum steering beyond instrumental causal networks, *Phys. Rev. Lett.* **120**, 140408 (2018).
- [32] I. Agresti, D. Poderini, L. Guerini, M. Mancusi, G. Carvacho, L. Aolita, D. Cavalcanti, R. Chaves, and F. Sciarrino, Experimental device-independent certified randomness generation with an instrumental causal structure, *Commun. Phys.* **3**, 110

- (2020).
- [33] X. Liu, Q. Chen, and O. Dahlsten, Inferring the arrow of time in quantum spatiotemporal correlations, *Phys. Rev. A* **109**, 032219 (2024).
- [34] E. Wolfe, A. Pozas-Kerstjens, M. Grinberg, D. Rosset, A. Acín, and M. Navascués, Quantum inflation: A general approach to quantum causal compatibility, *Phys. Rev. X* **11**, 021043 (2021).
- [35] R. Chaves, C. Majenz, and D. Gross, Information–theoretic implications of quantum causal structures, *Nat. Commun.* **6**, 5766 (2015).
- [36] C. Miquel, J. P. Paz, M. Saraceno, E. Knill, R. Laflamme, and C. Negrevergne, Interpretation of tomography and spectroscopy as dual forms of quantum computation, *Nature* **418**, 59 (2002).
- [37] Z. Zhang, X. Long, X. Zhao, Z. Lin, K. Tang, H. Liu, X. Yang, X. Nie, J. Wu, J. Li, T. Xin, K. Li, and D. Lu, Identifying abelian and non-abelian topological orders in the string-net model using a quantum scattering circuit, *Phys. Rev. A* **105**, L030402 (2022).
- [38] X. Liu, Y. Qiu, O. Dahlsten, and V. Vedral, Quantum causal inference with extremely light touch, *arXiv preprint arXiv:2303.10544* (2023).
- [39] H. Liu, X. Liu, Q. Chen, Y. Qiu, V. Vedral, X. Nie, O. Dahlsten, and D. Lu, Quantum causal inference via scattering circuits in NMR (2024).
- [40] C. Marletto, V. Vedral, S. Virzì, E. Rebufello, A. Avella, F. Piacentini, M. Gramegna, I. P. Degiovanni, and M. Genovese, Theoretical description and experimental simulation of quantum entanglement near open time-like curves via pseudo-density operators, *Nat. Commun.* **10**, 182 (2019).
- [41] C. Marletto, V. Vedral, S. Virzì, A. Avella, F. Piacentini, M. Gramegna, I. P. Degiovanni, and M. Genovese, Temporal teleportation with pseudo-density operators: How dynamics emerges from temporal entanglement, *Sci. Adv.* **7**, eabe4742 (2021).
- [42] X. Liu, Z. Jia, Y. Qiu, F. Li, and O. Dahlsten, Unification of spatiotemporal quantum formalisms: Mapping between process and pseudo-density matrices via multiple-time states, *New J. Phys.* **26**, 033008 (2024).
- [43] T. Zhang, O. Dahlsten, and V. Vedral, Different instances of time as different quantum modes: quantum states across space-time for continuous variables, *New J. Phys.* **22**, 023029 (2020).
- [44] C. Xi, X. Liu, H. Liu, K. Huang, X. Long, D. Ebler, X. Nie, O. Dahlsten, and D. Lu, Experimental validation of enhanced information capacity by quantum switch in accordance with thermodynamic laws, *Phys. Rev. Lett.* **133**, 040401 (2024).
- [45] A. Souza, I. Oliveira, and R. Sarthour, A scattering quantum circuit for measuring Bell’s time inequality: A nuclear magnetic resonance demonstration using maximally mixed states, *New J. Phys.* **13**, 053023 (2011).
- [46] X. Nie, B.-B. Wei, X. Chen, Z. Zhang, X. Zhao, C. Qiu, Y. Tian, Y. Ji, T. Xin, D. Lu, and J. Li, Experimental observation of equilibrium and dynamical quantum phase transitions via out-of-time-ordered correlators, *Phys. Rev. Lett.* **124**, 250601 (2020).